

A High-Frequency and Multi-Epoch VLBI Study of 3C 273

T.P. Krichbaum¹, D.A. Graham¹, A. Witzel¹, J.A. Zensus¹, A. Greve²,
M. Grewing², A. Marscher³, and A.J. Beasley⁴

(1) *Max-Planck-Institut für Radioastronomie, Bonn, Germany*

(2) *Institut de Radioastronomie Millimétrique, Grenoble, France*

(3) *Department of Astronomy, Boston University, Boston, USA*

(4) *National Radio Astronomy Observatory, Socorro, USA*

Abstract. We show results from a 7 year VLBI monitoring programme of 3C 273 at millimeter wavelengths. We find evidence for component acceleration, motion or rotation of fluid dynamical patterns, and an outburst-ejection relation between γ -ray flares and new jet components.

1. Introduction

VLBI imaging at millimeter wavelengths (mm-VLBI) gives highest angular resolution and facilitates direct studies of the self-absorbed jet base in AGN. For 3C 273 ($z = 0.158$) images with an angular resolution of up to $50 \mu\text{as}$ ($1 \mu\text{as} = 10^{-6}$ arcsec) are made at 86 GHz. This corresponds to a spatial scale of ~ 1000 Schwarzschild radii (for $M = 10^9 M_{\odot}$). The small observing beam allows to accurately determine positions of jet components. This facilitates detailed studies of the jet structure and kinematics near the nucleus, in particular with regard to the broad-band (radio to Gamma-ray) flux density variability and the birth of new ‘VLBI components’. Here we summarize new results from our multi epoch (1990 – 1997) and high observing frequency (15, 22, 43 and 86 GHz) VLBI monitoring.

2. Results

At sub-milliarcsecond resolution, 3C 273 shows a one sided core-jet structure of several milliarcseconds length. The jet breaks up into multiple VLBI components, which – when represented by Gaussian components – seem to separate at apparent superluminal speeds from the stationary assumed VLBI core. The cross-identification of the model-fit components, seen at different times and epochs, is facilitated by small (< 0.2 mas), and to first order negligible, opacity shifts of the component positions relative to the VLBI-core. Quasi-simultaneous data sets (cf. Fig. 1) demonstrate convincingly the reliability of the component identification, which results in a kinematic scenario, in which all detected jet components (C6 – C18) move steadily (without ‘jumps’ in position) away from the core (Fig. 4). For the components with enough data points at small (< 2 mas) and large (> 2 mas) core separations, quadratic fits to the radial motion $r(t)$ (but also for $x(t)$ –right ascension, and $y(t)$ –declination) represent the observations much better than linear fits. Thus the components seem to accelerate as they move out. The velocities range typically from $\beta_{app} = 4 - 8$ (for $H_0 = 100 \text{ km s}^{-1} \text{ Mpc}^{-1}$, $q_0 = 0.5$).

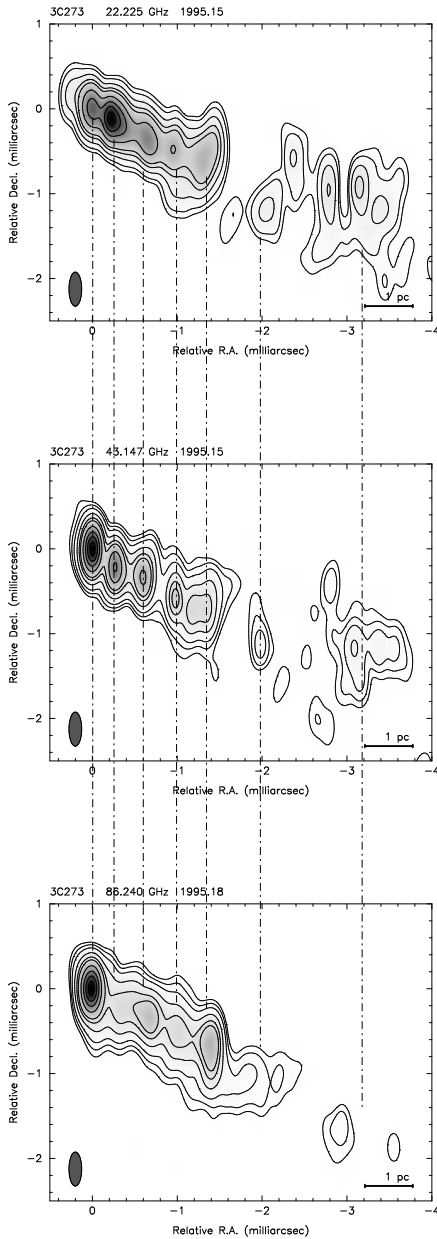


Fig. 1: 3C 273 at 22 GHz (top), 43 GHz (center), and 86 GHz (bottom) observed in 1995.15 – 1995.18. Contour levels are -0.5, 0.5, 1, 2, 5, 10, 15, 30, 50, 70, and 90% of the peak of 3.0 (top), 5.4 (center), and 4.7 Jy/beam (bottom). For the 22 GHz map, the 0.5% contour is omitted. The restoring beam is 0.4×0.15 mas in size, oriented at $pa = 0^\circ$. The maps are centered on the eastern component (the core), the dashed lines guide the eye and help to identify corresponding jet components.

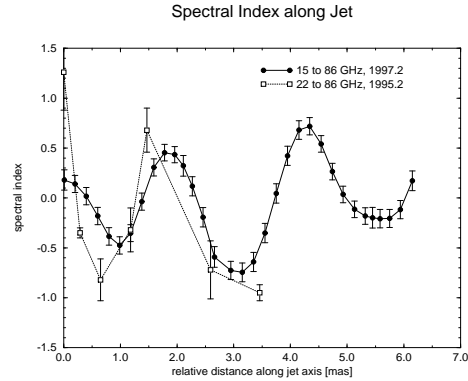


Fig. 2: Spectral index variations along the jet. For 1997 (circles, solid lines), the spectral index gradient is calculated directly from the intensity profiles of the maps at 15 and 86 GHz. For 1995 (squares, dashed line), the spectral indices were derived from Gaussian component model fits at 22 and 86 GHz. We note that during the time interval 1995 – 1997, different jet components occupied this jet region. The spectral profile along the jet, however, did not change significantly.

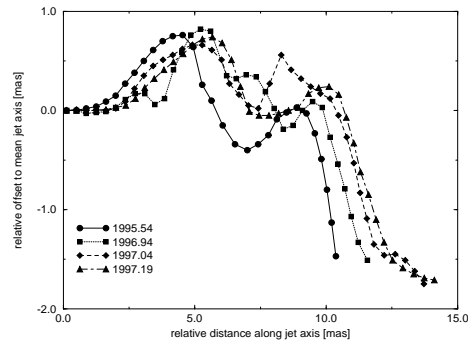


Fig. 3: The motion of the mean jet axis in the inner jet of 3C 273 at 15 GHz. Symbols denote for different epochs: 1995.54 (circles), 1996.94 (squares), 1997.04 (diamonds), and 1997.19 (triangles). The transverse oscillations of the ridge line are measured relative to a straight line oriented along $pa = 240^\circ$. We note the systematic longitudinal displacement of maxima and minima. This corresponds to an apparent pattern velocity of $\beta_{app} \simeq 4.2$, which is by a factor of up to 2 slower than the component motion.

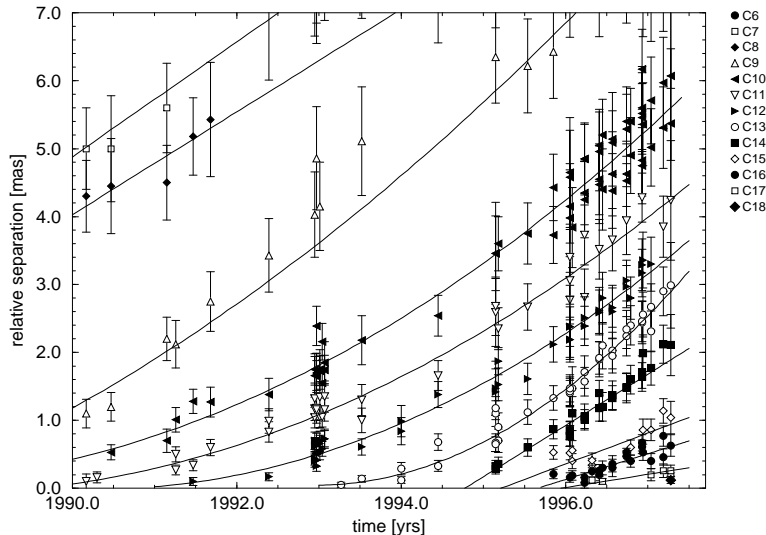


Fig. 4: Relative core separations $r(t)$ for the components C6 – C18. The legend on the right identifies symbols with VLBI components. The lines are least square fits to the data.

Dual-frequency maps obtained in 1995 (22/86 GHz) and 1997 (15/86 GHz) allow to measure the spectral index gradient along the jet (see Fig. 2). The spectrum oscillates between $-1.0 \leq \alpha \leq +0.5$ ($S_\nu \propto \nu^\alpha$). Most noteworthy, the spectral gradients did not change significantly over the 2 year time period, although different jet components occupied this jet region. Thus, the geometrical (eg. relativistic aberration) and/or the physical environment (pressure, density, B-field) in the jet must determine the observed properties of the VLBI components. Hence, the latter do not form ‘physical entities’, but seem to react to the physical conditions of the jet fluid.

Further evidence for a fluid dynamical interpretation comes from a study of the mean jet axis and the transverse width of the jet. Both oscillate quasi-sinusoidally on mas-scales. At 15 GHz, the variation of the ridge-line with time could be determined from 4 VLBA maps obtained during 1995 – 1997 (Fig. 3). The maxima and minima of the ridge-line are systematically displaced. This ‘longitudinal’ shift suggests motion with a pattern velocity of $\beta_{app} = 4.2$. The sinusoidal curvature of the jet axis, however, is more indicative for jet rotation rather than for longitudinal waves. Helical Kelvin-Helmholtz instabilities propagating in the jet sheath could mimic such rotation, which, when seen in projection, would explain also the spectral index oscillation in Figure 2.

For many AGN, a correlation between flux density variability and ejection of VLBI components is suggested. In 3C 273 we identified 13 jet components (C6 – C18) and traced their motion back to their ejection from the VLBI core. The typical measurement uncertainty for the ejection times t_0 ranges between 0.2 – 0.5 yr. In Figure 5 (left) we plot t_0 and the millimeter-variability (22 – 230 GHz). We also add the Gamma-ray detections of 3C 273 from EGRET. In Figure 5 (right) we plot the onset times of the mm-flares derived from these light curves (Türler et al. 1999) together with the VLBI ejection time (t_0) and the Gamma-ray fluxes. For each onset of a mm-flare, we find that a new jet component was ejected.

Although the time sampling of the Gamma-ray data is quite coarse, a relation between component ejection and high Gamma-ray flux appears very likely (note that each Gamma-detection already means higher than usual γ -brightness). From a more detailed analysis (Krichbaum et al. 2001) we obtain for the time lag between component ejection and onset of a mm-flare: $t_0 - t_0^{\text{mm}} = 0.1 \pm 0.2$ yr. If we assume that the observed peaks in the Gamma-ray light-curve are located near the times t_0^γ of flux density maxima, we obtain $t_0^\gamma - t_0^{\text{mm}} = 0.3 \pm 0.3$ yr. Although the Gamma-ray variability may be faster, this result is fully consistent with the more general finding of enhanced Gamma-ray fluxes mainly during the rising phase of millimeter flares. We therefore suggest the following tentative sequence of events: $t_0^{\text{mm}} \leq t_0 \leq t_0^\gamma$ – the onset of a millimeter flare is followed by the ejection of a new VLBI component and, either simultaneously or slightly time-delayed, an increase of the Gamma-ray flux. If we focus only on those VLBI components, which were ejected close to the main maxima of the Gamma-ray light-curve in Figure 5, we obtain time lags of $t_0^\gamma - t_0$ of ≤ 0.5 yr for C12, ≤ 0.9 yr for C13, ≤ 0.2 yr for C16 and ≤ 0.1 yr for C18. In all cases the Gamma-rays seem to peak a little later than the time of component ejection. With $\beta_{\text{app}} \simeq 4$ near the core, the Gamma-rays would then escape at a radius $r_\gamma \leq 0.1$ mas. This corresponds to $r_\gamma \leq 2000$ Schwarzschild radii (for a $10^9 M_\odot$ black hole) or $\leq 6 \cdot 10^{17}$ cm, consistent with theoretical expectations, in which Gamma-rays escape the horizon of photon-photon pair production at separations of a few hundred to a few thousand Schwarzschild radii.

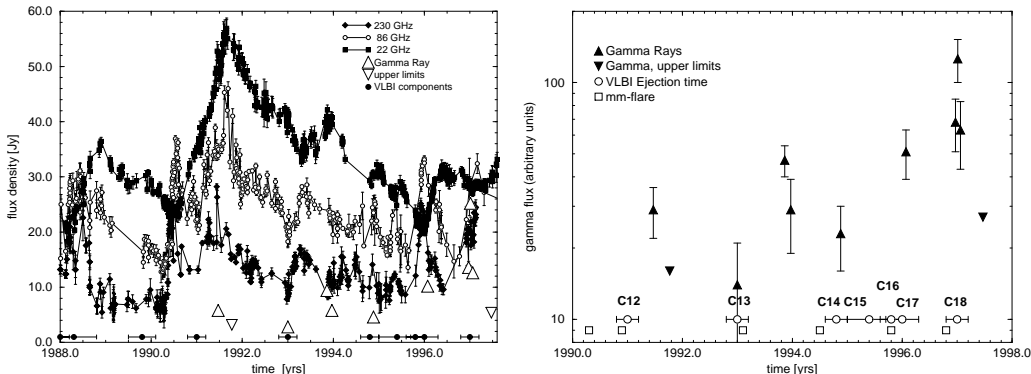


Fig. 5: Left: Flux density variations at 230 GHz (filled diamonds), 86 GHz (open circles) and 22 GHz (filled squares). Upward oriented triangles denote Gamma-ray fluxes from EGRET, downward oriented triangles are upper limits. The extrapolated ejection times of the VLBI components and their uncertainties are indicated by filled circles with horizontal bars along the time axis. Right: Broad-band flux density activity and component ejection. VLBI component ejection (open circles), Gamma-ray fluxes (triangles, downward oriented for upper limits) and onset-times for the millimeter flares (open squares, from Türler et al. 1999). Labels denote the component identification from VLBI.

References:

- Türler M., Courvoisier T.J.-L., & Paltani S., ‘Modelling the submillimeter-to-radio flaring behaviour of 3C 273’, 1999, *A&A*, **349**, p. 45–54.
 Krichbaum T.P., et al., ‘High Frequency VLBI Observations of 3C 273’, 2001, *A&A*, submitted.